Applied Catalysis B: Environmental 165 (2015) 620–627

Contents lists available at ScienceDirect

Applied Catalysis B: Environmental

journal homepage: www.elsevier.com/locate/apcatb

Shift from heterogeneous to homogeneous catalysis during resorcinol degradation using the solar photo-Fenton process initiated at circumneutral pH

José Fernando Barona[a], Diego Fernando Morales[a], Luis Ferney González-Bahamón[a], Cesar Pulgarín[b,**], Luis Norberto Benítez[a,*]

[a] Universidad del Valle, Grupo de Investigación en Procesos Avanzados de Oxidación (GAOX), A. A. 25360 Cali, Colombia
[b] Ecole Polytechnique Fédérale de Lausanne (EPFL), Institute of Chemical Science and Engineering, GPAO Station 6, CH-1015 Lausanne, Switzerland

ARTICLE INFO

Article history:
Received 18 May 2014
Received in revised form 3 October 2014
Accepted 21 October 2014
Available online 1 November 2014

Keywords:
Heterogeneous/homogeneous photo-Fenton
Photo-Fenton at circumneutral pH
Resorcinol degradation
Photo-Fenton mechanistic path at circumneutral pH

ABSTRACT

The photo-Fenton process ($Fe^{2+,3+}/H_2O_2/h\nu$) is known to degrade aqueous organic compounds at acidic pHs. Nevertheless, recent studies have shown that this process also occurs at circumneutral pHs. Dihydroxybenzene isomers (i.e., resorcinol, hydroquinone and catechol) were selected as models of degradation by-products of natural organic matter and were degraded in water via the solar photo-Fenton process in a compound parabolic collector (CPC). The experiments were carried out at neutral pH and with 0.7 and 40.0 mg L^{-1} of iron and H_2O_2, respectively. Despite sharing a similar chemical structure as the other two isomers, resorcinol was more recalcitrant to degradation under these conditions. Thus, we conducted a detailed study of this compound's transformation through the photo-Fenton process. The effects of initial pH (5.0, 6.0 and 7.4) on resorcinol degradation were investigated, and in all experiments, pH, total organic carbon (TOC), resorcinol, dissolved iron forms and H_2O_2 were monitored. The results led us to consider that a photo-Fenton system at circumneutral pH follows a different mechanism than the pathway that is generally accepted for acidic pH values. A photo-Fenton process initiated at neutral pH is mainly heterogeneous; however, as the pH progressively decreases due to the generation of acidic by-products, the process becomes more homogeneous, and the degradation rate increases concomitantly. The pH also dramatically drops to approximately 5.7. A mechanism is proposed to explain the key shift from heterogeneous towards homogeneous photo-Fenton degradation processes.

1. Introduction

Advanced oxidation processes (AOPs) have garnered great interest as promising alternatives for the treatment of water containing organic pollutants and NOM (natural organic matter) [1–7]. These processes are characterised by the generation of highly reactive hydroxyl radicals ($HO^{\bullet}$), which are suitable for use in rapid and non-selective reactions with organic compounds [8–13]. Among the AOPs, the photo-assisted Fenton (Fe^{2+}/H_2O_2) reaction at acidic pH is a homogeneous catalytic process that is used to generate $HO^{\bullet}$, as shown in Eqs. (1) and (2)

$$Fe^{2+} + H_2O_2 \rightarrow Fe^{3+} + HO^{\bullet} + HO^{-} \quad (1)$$

$$[Fe(OH)]^{2+} + h\nu \rightarrow Fe^{2+} + HO^{\bullet} + H^{+} \quad (2)$$

Nevertheless, the efficiency of the photo-Fenton process in organic matter degradation is strongly dependent on pH; the optimum pH value is approximately 3.0 [14]. Indeed, when the pH is acidic, aquo-complex deprotonation is not favoured, and iron hydroxylation is limited, allowing the formation of partially hydrolysed soluble iron species such as $[Fe(OH)(H_2O)_5]^{2+}$, which are active under UV-A and visible solar light [15,16]. In photo-Fenton processes under acidic conditions, the Fe/H_2O_2 concentration ratio oscillates between 1:10 and 1:300, depending on the target organic compound [17–21]. However, previous studies have reported that a starting pH of 5.0 was sufficient to degrade the NOM of rivers through the photo-Fenton process [22,23]. Similar results were obtained during the degradation of organic pollutants in wastewaters at neutral and circumneutral pHs [24–31], but no proposed mechanism explaining the reactivity of the photo-Fenton process when initiated at near-neutral pH values is available.

* Corresponding author. Tel.: +57 2 3393248.
** Corresponding author. Tel.: +41 21 6934720.
E-mail addresses: cesar.pulgarin@epfl.ch (C. Pulgarín), luis.benitez@correounivalle.edu.co (L.N. Benítez).

http://dx.doi.org/10.1016/j.apcatb.2014.10.053
0926-3373/

Several authors have demonstrated the presence of ferrous species such as $[Fe(H_2O)_6]^{2+}$, $[Fe(OH)(H_2O)_5]^{+}$ and $[Fe(OH)_2(H_2O)_4]$ at pH values between 4.0 and 8.0 as well as fast ferrous species oxidation by dissolved oxygen in water [32–35].

In the absence of ligands other than water, iron cations generate hexacoordinated aquo-complexes (e.g., $[Fe(H_2O)_6]^{2+/3+}$), in which the polarisation of water molecules is strongly dependent on the charge and size of the cation. This polarisation makes the ferric aquo-complexes more acidic than the ferrous complexes; therefore, the deprotonation (or hydroxylation) of $Fe^{2+/3+}$ complexes occurs at different pH ranges (pH 7–9 and 1–5 for Fe^{2+} and Fe^{3+}, respectively). Jolivet et al. [36] reported that iron zero-charge aquohydroxo complexes are precursors of species in the solid state. Zero-charge ferrous complexes, e.g., $Fe(OH)_2(H_2O)_4$ can be formed at circumneutral pH, but their high lability towards oxidation quickly leads to solid ferric compounds such as green rusts, magnetite, goethite, lepidocrocite or ferroxyhyte, depending on the physicochemical conditions, which include the presence of organic and inorganic ligands [36]. In experiments carried out in this work, the photo-Fenton process is applied to the degradation of a siderophore (catechol), which chelates iron in solution, even at neutral pHs. Therefore, in the Fenton processes that begin at neutral pHs, both homogeneous and heterogeneous catalyses are involved, and the relative contribution of the catalysis type to the overall degradation of the target compound depends on the pH and the oxidation by-products, which change during the process. By accounting for the above considerations, the photo-Fenton process at circumneutral pH follows a different path than the generally accepted pathway for pH ~ 3 (Eqs. (1) and (2)). The goal of this work is to better understand the degradation mechanism of the most recalcitrant dihydroxybenzene isomer (resorcinol) under a solar photo-Fenton process initiated at near-neutral pH.

2. Experimental

2.1. Reagents

Resorcinol, catechol and hydroquinone (98%, Carlo Erba); H_2O_2 (30%, Riedel-de Haën); $FeSO_4{\cdot}7H_2O$ (98%, Merck); NaCl (99%, Merck), Na_2SO_3 (99%, Merck), and NaOH (99%, Merck) were used as received. Deionised (18.2 MΩ cm) and distilled water were used for standard solutions and photo-catalytic tests, respectively.

2.2. Analytical methods

The concentrations of dihydroxybenzene isomers were determined by high performance liquid chromatography (HPLC 2010AHT Shimadzu) outfitted with a C18 column (Alltech, 5 μm particle size, 3.9 mm internal diameter and 250 mm length) and detection at 254 nm. For resorcinol, the mobile phase was methanol–water (50:50) at 1.0 mL min^{-1}, and for catechol and hydroquinone, the mobile phase was a mixture of methanol–aqueous H_3PO_4 (20:80) buffered at pH 2.8, with a flow rate of 0.6 mL min^{-1} was used. Total organic carbon was measured using a TOC analyser (TOC VCPH Shimadzu). Qualitative monitoring of the H_2O_2 concentration was realised using Merkoquant (Merck) peroxide analytical test strips, while the H_2O_2 quantitative analysis was realised via spectrophotometry at 410 nm using a titanium (IV) oxysulphate solution (modified method, DIN 38 402 H15). The pH was measured with a pH-metre (Metrohm 827 pH-lab) outfitted with a glass electrode. Total iron was measured by atomic absorption spectroscopy (AAs 100 Perkin Elmer), and iron complexes (Fe-ferrozine and Fe-other) were measured by molecular absorption spectroscopy (UV–vis 1700 Shimadzu). Additionally, the bonding structure in particle samples was analysed by Fourier transform infrared spectroscopy (6700 FT-IR Nicolet). Pressed pellets composed of 80 mg of KBr and 0.8 mg of powdered samples were used.

2.3. Photo-catalytic process

Deionised water was spiked with the target organic substance (15 mg L^{-1}) and iron (0.7 mg L^{-1}), and the pH was adjusted to 7.0 with NaOH (0.1 mol L^{-1}). H_2O_2 was added to 1 L of this solution (to obtain 40 mg L^{-1}) in a laboratory-scale CPC reactor (see below). The solution was then exposed to radiation provided by Suntest Atlas XLS+ (300–800 nm, irradiance = 500 W m^{-2}). To degrade resorcinol by the solar Fenton process, the solutions were prepared in 25 L of distilled water at the above-mentioned concentrations and at three pH values (5.0, 6.0 and 7.4) and then exposed to light in Cali, Colombia between February and July 2010. The CPC consisted of four Pyrex tubes (1.5 m length, 3.2 cm internal diameter and 3.6 cm external diameter) that were placed over a reflective surface of anodised aluminium (the laboratory-scale CPC reactor varied only in length (10 cm) and in the tube number (1)) with a 3° inclination, corresponding to the latitude of the site. Moreover, the solutions (25 L) were circulated at 50 L min^{-1} through the reactor which was comprised of a 25 L tank connected to a centrifugal pump (the dissolved oxygen concentration was ~6.0 mg L^{-1} at 25 °C). The CPC reactor reached temperatures of 30–42 °C during the experiments, and the illuminated volume was 4.8 L. UV solar irradiance was measured using a radiometer that was sensitive between 300 and 400 nm (ACADUS S2004 with a controller LS-3300) and was mounted at the same angle as the CPC reactor. The accumulated energy incident on the photo-reactor for each sample during the experiment per volume unit ($Quv,_n$) was assessed by the application of Eq. (3) [37].

$$Quv,_n = Quv,_{n-1} + \Delta t_n UV_{G,n}\left[\frac{A_{CPC}}{V_{TOT}}\right], \quad \Delta t_n = t_n - t_{n-1} \tag{3}$$

where t_n is the experimental time; V_{TOT} is the reactor volume (4.8 L); A_{CPC} is the illuminated surface of the collector (0.61 m^2); $UV_{G,n}$ is the average of the global UV radiation during Δt_n; and $Quv,_n$, is the accumulated energy (per unit of volume, kJ L^{-1}) incident on the reactor.

Samples (60 mL) were taken at various intervals during the experiments to analyse the pH, iron content, resorcinol content, TOC, and hydrogen peroxide concentration. The catalytic reaction in each sample was quenched with 0.1 mL of 1.2 mol L^{-1} Na_2SO_3 before analysing the different parameters. For Fe^{2+} determination, a complexing agent (ferrozine) was added in the presence of light, and the sample vial was immediately covered for 15 min. Subsequently, complexed iron was spectrophotometrically quantified at 550 nm. All catalytic experiments were carried out in triplicate, and the RSD were <8%.

3. Results and discussion

3.1. Comparison of dihydroxybenzene isomer degradation kinetics

Fig. 1 shows the degradation and mineralisation of dihydroxybenzene isomers (resorcinol, hydroquinone and catechol) when the photo-Fenton process was initiated at neutral pH with 40 mg L^{-1} of H_2O_2 and 0.7 mg L^{-1} of Fe. Resorcinol is the most recalcitrant isomer. After 4 h of treatment, resorcinol was not fully transformed, and negligible mineralisation was achieved. Conversely, the other isomers were degraded very quickly and mineralised at high rates. Notably, the pH trends were similar for the degradation of all isomers: the conditions became acidic as the organic target

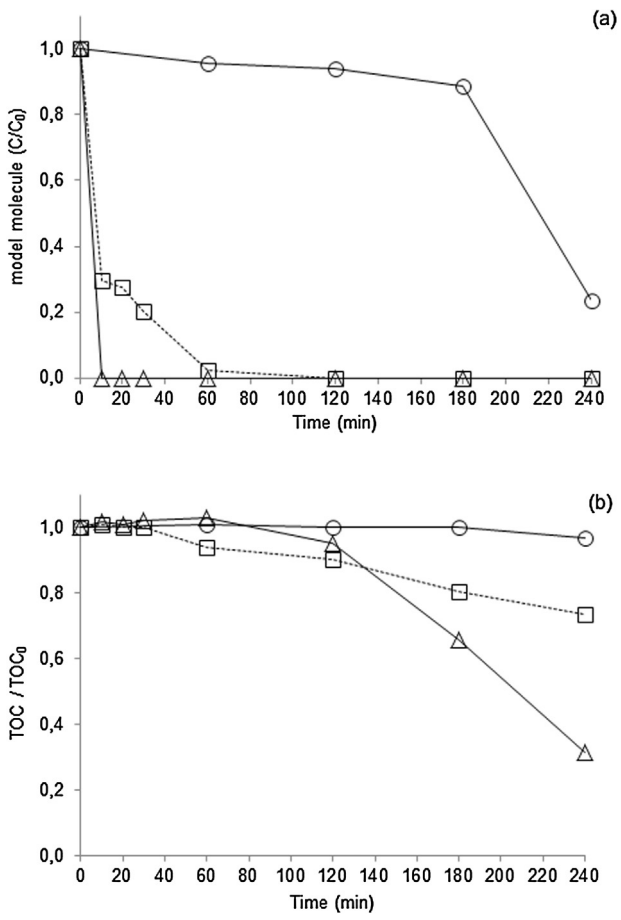

Fig. 1. Degradation (a) and mineralisation (b) of dihydroxybenzene isomers (resorcinol (○), hydroquinone (△) and catechol (□)) during the photo-Fenton process. $[Fe^{2+}]_0 = 0.7\ mg\ L^{-1}$, $[H_2O_2]_0 = 40\ mg\ L^{-1}$, pH_0 7.0 and 15.0 mg L^{-1} of the organic compound.

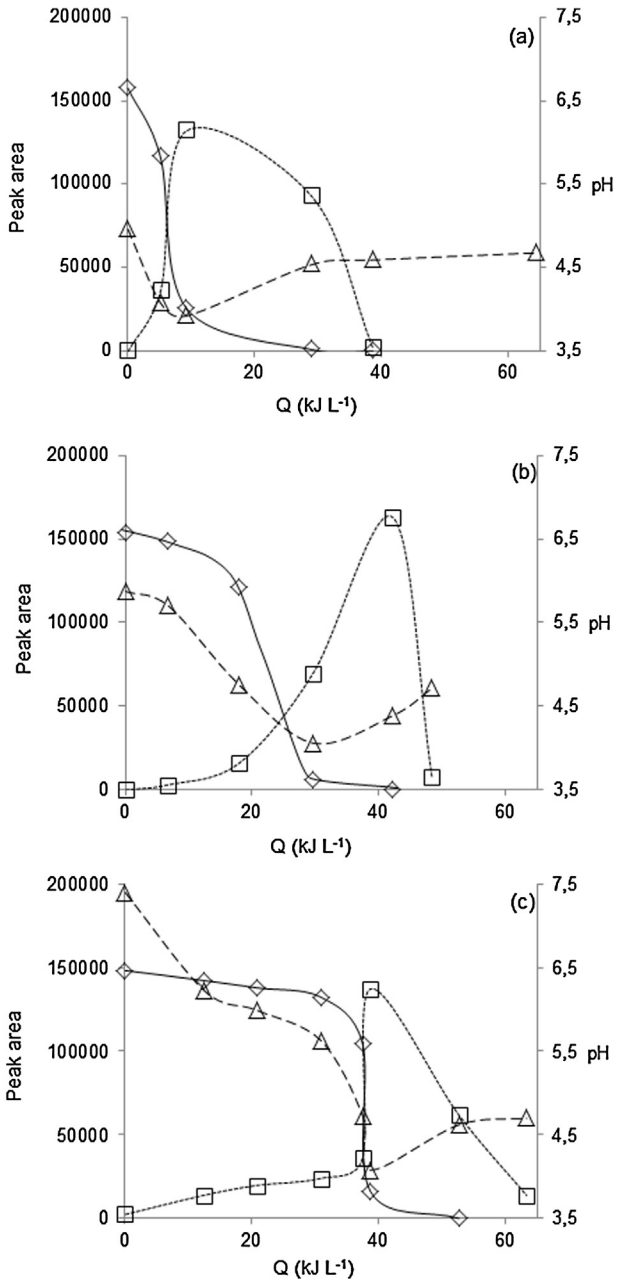

Fig. 2. Solar photo-Fenton treatment of aqueous resorcinol (15 mg L^{-1}) in CPC, $[Fe^{2+}]_0 = 0.7\ mg\ L^{-1}$, and $[H_2O_2]_0 = 40\ mg\ L^{-1}$ at an initial pH of 5.0 (a), 6.0 (b), and 7.4 (c). pH evolution (△), resorcinol degradation (◊) and accumulated by-products (□).

degradation progressed. For hydroquinone and catechol, lower pH values (~4.6) were obtained at 120 min; however, for resorcinol degradation, this pH was achieved only after 240 min (results not shown). Therefore, under these conditions, the degradation kinetics of the three compounds are markedly different.

In addition to photo-Fenton degradation, hydroquinone undergoes rapid transformation to benzoquinone in a process promoted by Fe^{3+}, which is simultaneously reduced [38]. After the iron reacts with H_2O_2, thereby returning to its oxidised state and producing hydroxyl radical (Fenton reaction), the resulting radical contributes to hydroquinone conversion. Because catechol is a siderophore, it can keep the iron in solution via complexation; therefore, oxidation of the organic target occurs either by ligand-to-metal charge transfer (LMCT) or by photo-Fenton processes [38–40]. In contrast, resorcinol degradation was only achieved through the photo-Fenton process. However, after 3 h of treatment, an increase in the resorcinol degradation rate was observed; therefore, it was necessary to perform a systematic study of resorcinol degradation at neutral pH values to understand this process.

3.2. Evolution and the effect of pH during resorcinol degradation

Fig. 2 illustrates the pH evolution, resorcinol degradation and overall formation/decay of by-products during the solar photo-Fenton treatment of aqueous resorcinol at different initial pH values. Although a larger $Quv,_n$ was required to degrade resorcinol at pH 7.4 than at pH 6.0 and therefore also at pH 5.0, the general trend of resorcinol degradation and by-product accumulation were similar for all pHs. The chromatographic analysis showed a decrease in resorcinol with an accumulation of by-products. First, the pH decreased to 4.0 as a result of the acidic nature of the by-products [41], and then the pH increased to 4.6 (Fig. 2 (△)) due to the mineralisation of these compounds (Fig. 3).

Fig. 3 shows the evolution of organic carbon (TOC/TOC_0) during resorcinol degradation by the photo-Fenton process at different initial pH values. Up to 85% resorcinol mineralisation was reached when the photo-Fenton process was initiated at pH 5.0, 6.0 and 7.4; a greater $Quv,_n$ was required at pH 7.4. In contrast, the resorcinol mineralisation by Fenton and solar light/H_2O_2 processes initiated at pH 5.5, 6.5 and 7.5 did not exceed 30% and was even null at pH 7.5.

Clearly, resorcinol degradation and especially its mineralisation rates (Figs. 2 and 3) strongly depend on the initial pH. The

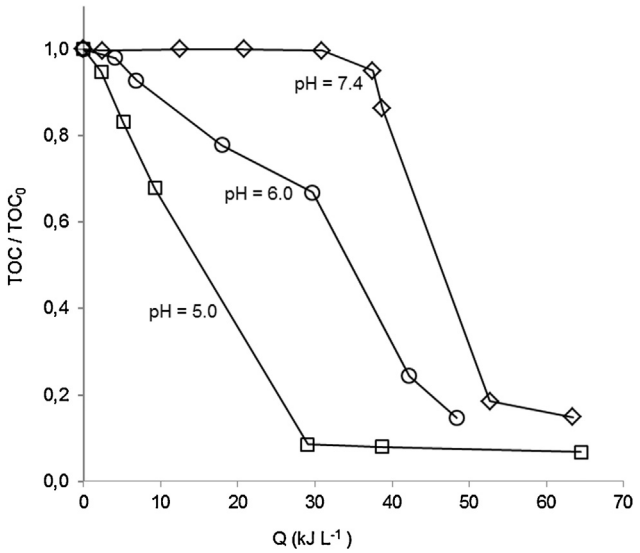

Fig. 3. TOC evolution during resorcinol degradation in a CPC by photo-Fenton treatment at different initial pH values. [Resorcinol] = 15 mg L^{-1}, $[Fe^{2+}]_0$ = 0.7 mg L^{-1} and $[H_2O_2]_0$ = 40 mg L^{-1}.

formation of acidic by-products during treatment accelerates substrate degradation, and the differences in resorcinol degradation, by-product accumulation/degradation (Fig. 2), and mineralisation (Fig. 3) at different initial pH values are all strongly correlated with the time required to reach pH ~ 5.7 in each case. At that point, the degradation rates sharply accelerate, suggesting that resorcinol degradation and mineralisation are primarily catalysed by iron–carboxylic acid complexes that are photo-active at pH ≤ 5.7. Ligands in the latter complexes are aliphatic acids resulting from the oxidation of resorcinol, and indeed, five aliphatic acids were identified during resorcinol degradation by the photo-Fenton process at different initial pH values (see Fig. 4 to observe the chromatogram obtained at an initial pH of 6.0).

The pH decrease is mainly due to accumulated acetic acid (approximately 24 mg L^{-1}), which is theoretically sufficient to reach a pH of 4.0. Furthermore, it has been reported [42–47] that the photoactive iron-acetate complexes that are formed favour a homogenous catalytic process.

3.3. Iron species in the photo-Fenton process at circumneutral pH in the absence of resorcinol

Fig. 5 shows the decay of the $[Fe^{2+}]/[Fe^{2+}]_0$ ratio in aqueous systems at pH 6.9 and 7.4 with or without the addition of H_2O_2. In the absence of H_2O_2 (Fig. 5), a remarkable difference in the formation rate of iron precipitate was observed between pH 6.9 and 7.4 that was due to the oxidation of Fe^{2+} by dissolved O_2. Morgan and Lahav [33] reported that at circumneutral pH and Fe^{2+} concentrations below 1 mg L^{-1}, soluble iron species are formed in water (Eqs. (4)–(6)) before undergoing oxidation by O_2 (Eqs. (7)–(9)). Under these conditions, hydrolysed species are more readily oxidised.

$$Fe^{2+} + 6H_2O \rightarrow [Fe(H_2O)_6]^{2+} \quad (4)$$

$$[Fe(H_2O)_6]^{2+} + HO^- \rightarrow [Fe(OH)(H_2O)_5]^+ + H_2O \quad (5)$$

$$[Fe(OH)(H_2O)_5]^+ + HO^- \rightarrow [Fe(OH)_2(H_2O)_4]_{(aq)} + H_2O \quad (6)$$

$$[Fe(H_2O)_6]^{2+} + O_2 \rightarrow [Fe(H_2O)_6]^{3+} + O_2^{\bullet -} \quad (7)$$

$$[Fe(OH)(H_2O)_5]^+ + O_2 \rightarrow [Fe(OH)(H_2O)_5]^{2+} + O_2^{\bullet -} \quad (8)$$

$$[Fe(OH)_2(H_2O)_4]_{(aq)} + O_2 \rightarrow [Fe(OH)_2(H_2O)_4]^+ + O_2^{\bullet -} \quad (9)$$

Fig. 5 (—) shows that shortly after of the addition of H_2O_2, soluble Fe^{2+} was not detected, regardless of the pH of the system. H_2O_2 favours the fast generation of insoluble species such as hematite, magnetite, goethite and lepidocrocite, most likely after the formation of meta-stable ferrous–ferric species (Eqs. (10) and (11)) [36]. Therefore, the activity of the photo-Fenton system at circumneutral pH is limited because the soluble iron concentration is negligible unless complexing organic substances are initially present or generated in situ.

$$4[Fe(OH)_2(H_2O)_4]_{(aq)} \rightarrow [Fe_4(OH)_8(H_2O)_8]_{(s)} + 8H_2O \quad (10)$$

$$[Fe_4(OH)_8(H_2O)_8]_{(s)} + O_2 \rightarrow 4FeOOH_{(s)} + 10H_2O \quad (11)$$

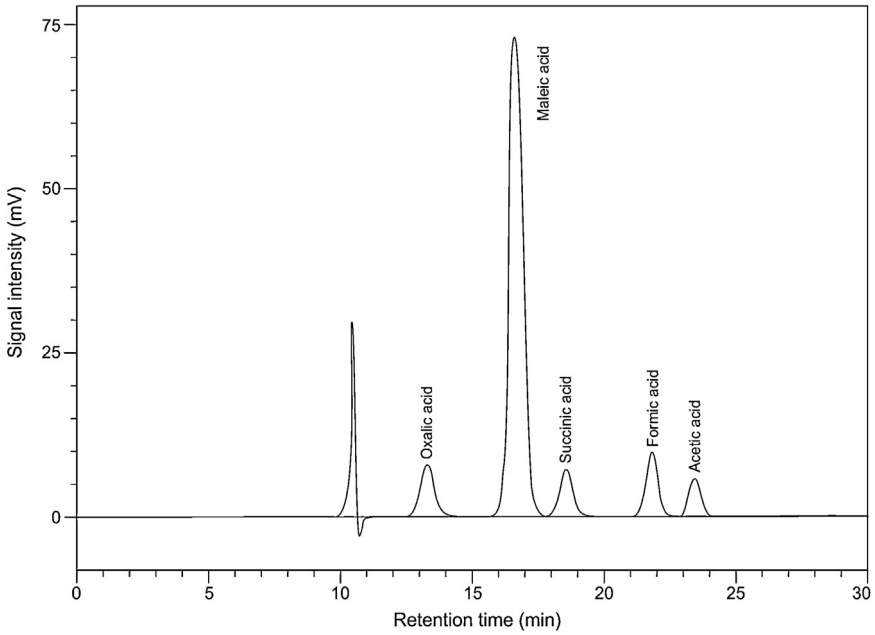

Fig. 4. Chromatogram of by-products obtained during resorcinol degradation (15 mg L^{-1}) by the solar-photo Fenton process at an initial pH of 6.0. $[Fe^{2+}]_0$ = 0.7 mg L^{-1}, $[H_2O_2]_0$ = 40 mg L^{-1} and Q = 40 kJ L^{-1}.

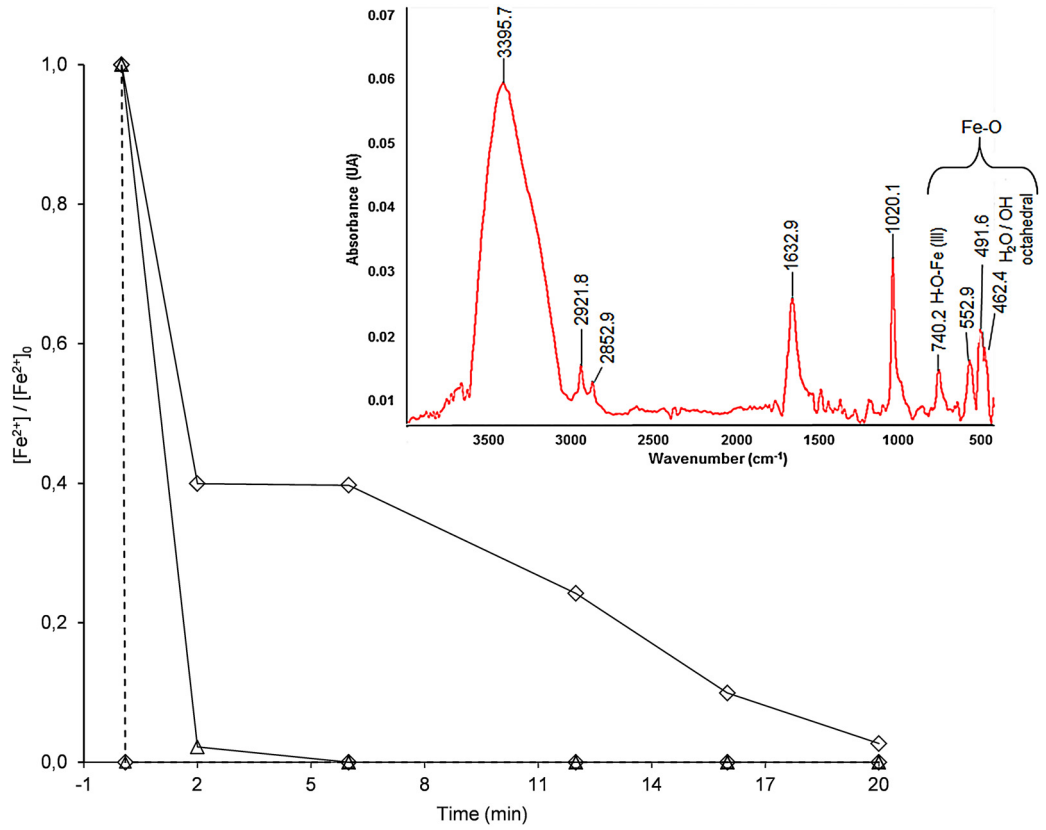

Fig. 5. Fe^{2+} remaining in the solution at an initial pH of 6.9 (◊) and 7.4 (△), with (—) and without (—) 40 mg L^{-1} H_2O_2. $[Fe^{2+}]_0$ = 0.7 mg L^{-1}. Dissolved oxygen (DO) approximately 6.0 mg L^{-1} at 25 °C. Inset: IR spectrum of ferric precipitates obtained after 30 min of treatment (pH 7.4).

The precipitated iron species of the experiments carried out at pH 6.0 and 7.4 in the absence of H_2O_2 and resorcinol were collected after 30 min for infrared (IR) analysis. The inset in Fig. 5 shows the IR spectrum of the sample obtained at pH 7.4; both IR spectra were similar.

The observed vibration bands are consistent with the typical IR spectra for iron oxide or oxyhydroxide, and the absorption bands at 3395 and 1633 cm^{-1} confirm the presence of water in the coordination sphere of the metal. The vibration modes of water are observed at 3766, 3652 and 1595 cm^{-1}, but they are shifted as a result of the HO–Fe interaction [48]. The absorption signals between 450 and 700 cm^{-1} are produced by Fe–O stretching in either oxides or oxyhydroxide, the band at 740 cm^{-1} is caused by the H–O–Fe (III) interaction, and the intense band at 491 cm^{-1} confirms the octahedral positions of the H_2O and OH groups in the ferric complexes [49,50]. Furthermore, the band at 1020 cm^{-1} is produced by the HO–Fe interaction in the (0 1 0) plane bending of lepidocrocite (γ-FeOOH) [51,52].

The precipitates obtained at pH 6.0 and 7.4 were yellow and brown, respectively; this colour variation is due to the different Fe:OH ratios in the solid caused by the final pH of the solution because other parameters affecting the surface area and morphologies (temperature, time of hydrolysis and oxidation process) were controlled [53]. The IR spectra indicate that the insoluble iron species formed in the studied photo-Fenton process (pH ≥ 5.7) are mainly oxyhydroxide alone or mixed as goethite (α-FeOOH) and lepidocrocite (γ-FeOOH).

3.4. Iron species in the photo-Fenton process at circumneutral pH in the presence of resorcinol

Fig. 6 shows the evolution of dissolved Fe^{2+} during aqueous resorcinol degradation through the solar photo-Fenton process.

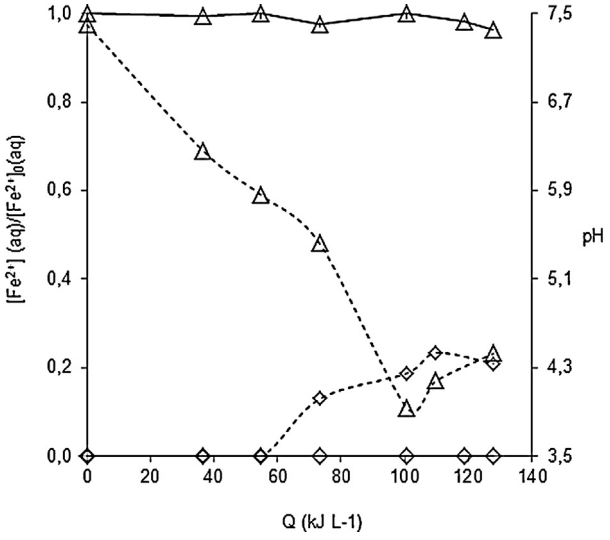

Fig. 6. Fe^{2+} in solution (◊) and pH evolution (△) during the photo-Fenton process at an initial pH of 7.5. Normal evolution of pH (—) and pH controlled at 7.4 via the continuous addition of NaOH (—). $[Fe^{2+}]_0$ = 0.7 mg L^{-1}, [resorcinol] = 15 mg L^{-1} and $[H_2O_2]_0$ = 40 mg L^{-1}.

When an initial pH of 7.5 was maintained by the continuous addition of NaOH throughout the reaction period (–△–), the dissolved Fe^{2+} concentration was negligible (–◊–). In contrast, 20% of the Fe^{2+} was dissolved when the pH was not controlled and allowed to drift to pH ~ 3.7 (–△–).

Fig. 6 shows that the fraction of Fe^{2+} in solution (–◊–) is favoured by (a) the pH dropping below 5.7 (–△–) due to the acidic nature of the resorcinol photo-degradation by-products (the decreased pH

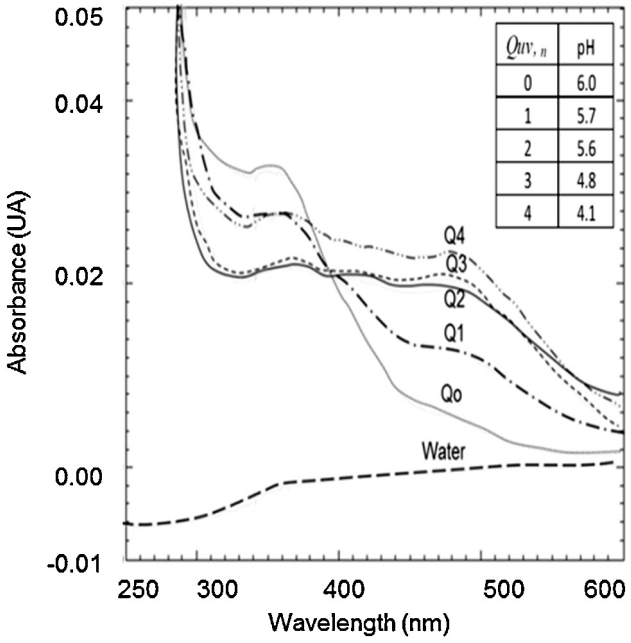

Fig. 7. Molecular absorption spectra of the filtered solutions at different $Quv,_n$ (Q_0 = 0.0, Q_1 = 4.1, Q_2 = 6.8, Q_3 = 17.9, and Q_4 = 29.6 kJ L^{-1}) during resorcinol degradation by the photo-Fenton process at an initial pH of 6.0. $[Fe^{2+}]_0$ = 0.7 mg L^{-1}, [resorcinol] = 15 mg L^{-1} and $[H_2O_2]_0$ = 40 mg L^{-1}.

slows the rate of Fe^{2+} oxidation by O_2) (Eq. (9)) [25]; and (b) the by-products functioning as polydentate ligands to form complexes with ferric ions (Eq. (12)), thereby allowing their solubilisation. Some of these complexes absorb in the near-UV and visible regions, inducing a LMCT to produce Fe^{2+} and ligand radicals (Eq. (13)) [54]. When the pH drops to approximately 5.7, Fe^{2+} begins to appear in the solution, and the photo-catalytic process shifts from heterogeneous towards homogeneous. Under homogeneous conditions, a significant enhancement of the photo-catalytic cycle ($Fe^{2+} \Leftrightarrow Fe^{3+}$) leads to a dramatic increase in hydroxyl radical production (Eq. (1)) and resorcinol degradation (Fig. 2).

3.5. Soluble photo-active iron complexes appearing during resorcinol degradation

UV–vis absorption spectra taken during aqueous resorcinol degradation by the solar photo-Fenton process at an initial pH of 6.0 are shown in Fig. 7. The spectra exhibit an absorption band at approximately 490 nm that increases in intensity as the pH decreases (Fig. 7, inserted table).

The absorption band at approximately 490 nm is due to the soluble compounds that were formed during the photo-catalytic process. The intensity of this band is correlated with a lower pH, indicating that the acidic by-products formed from resorcinol photo-degradation can form photo-active complexes with Fe^{3+}. In fact, some authors have reported that by-products such as oxalates can enter the Fe^{3+} coordination sphere and form soluble complexes (Eqs. (12) and (13)) [42,43], and these photo-active ferric complexes lead to an increase in ferrous ions in solution (Fig. 6, –◊–). Indeed, when pH ~ 5.7 is reached, soluble ferric complexes are formed, thereby preventing Fe^{3+} precipitation. In addition, the photo-excitation of Fe^{3+} complexes via a LMCT leads to the production of Fe^{2+}, which is required for the rapid homogeneous photo-Fenton process.

$$[Fe(H_2O)_6]^{3+} + 3[C_2O_4]^{2-} \rightarrow [Fe(C_2O_4)_3]^{3-} + 6H_2O \quad (12)$$

$$[Fe(C_2O_4)_3]^{3-} + h\nu \rightarrow Fe^{2+} + 2(C_2O_4)^{2-} + C_2O_4^{\bullet -} \quad (13)$$

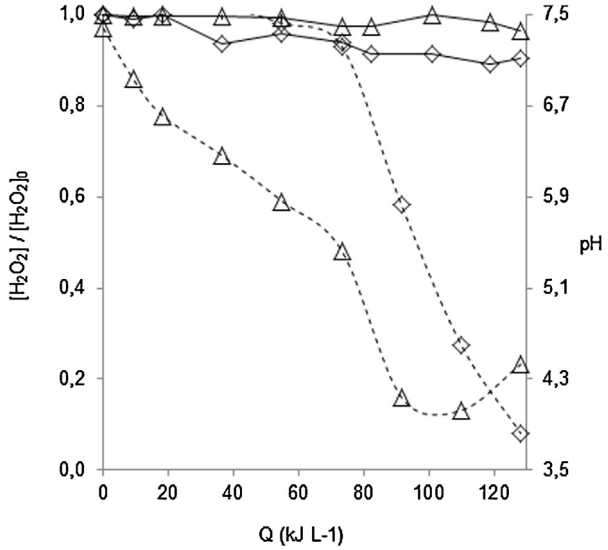

Fig. 8. Consumption of H_2O_2 (◊) and pH evolution (△) during the photo-Fenton process at an initial pH of 7.5. Normal evolution of pH (—) and controlled pH by the continuous addition of NaOH (—). $[Fe^{2+}]_0$ = 0.7 mg L^{-1}, [resorcinol] = 15 mg L^{-1} and $[H_2O_2]_0$ = 40 mg L^{-1}.

3.6. Hydrogen peroxide consumption during the photo-Fenton process at pH 7.5 in the presence of resorcinol

The hydrogen peroxide consumption during aqueous resorcinol degradation by the solar photo-Fenton process is dependent on the initial pH. The consumption at pH 6.0 was higher than that at pH 7.4, while the consumption was greater at pH 5.0 than at pH 6.0. Fig. 8 shows that when the pH was maintained at 7.5 (–△–) via the continuous addition of NaOH, H_2O_2 consumption was less than 10% of the 40 mg L^{-1} that was initially added (–◊–). In contrast, if the initial pH of 7.5 was not controlled and was allowed to spontaneously drift (–△–), the H_2O_2 consumption increased to 90% during the same reaction period (–◊–). However, in the latter case, faster hydrogen peroxide consumption was observed after the pH reached a value near 5.7, at which point, the homogeneous photo-Fenton process began to predominate.

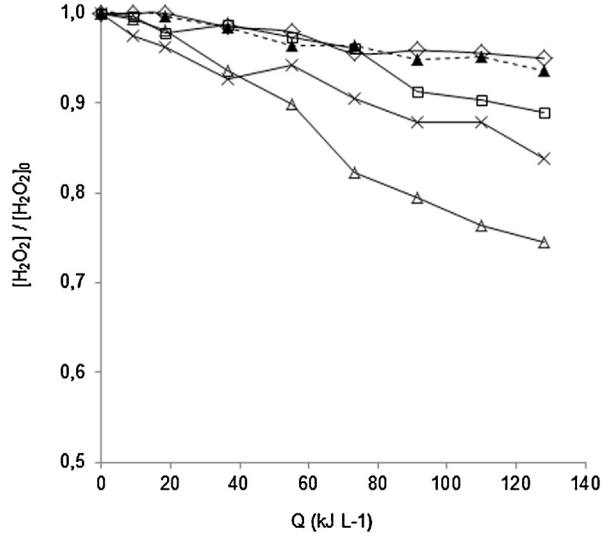

Fig. 9. Consumption of H_2O_2 during photo-Fenton (—) and Fenton (—) processes in the absence of resorcinol with a controlled pH at 7.5 by the continuous addition of NaOH. $[H_2O_2]_0$ = 40.0 mg L^{-1}, $[Fe]_0$ = 0.7 (◊), 1.4 (□), 2.8 (x) and 3.1 (△ and ▲) mg L^{-1}.

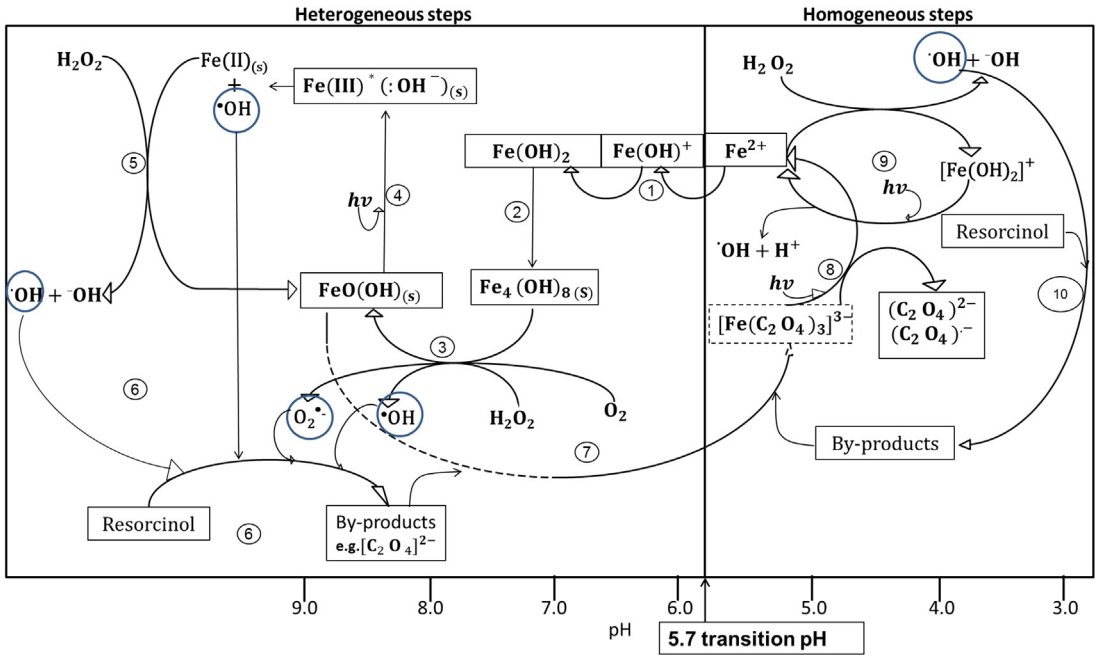

Fig. 10. Mechanisms involved and transition between heterogeneous and homogeneous photo-Fenton processes during resorcinol degradation.

Fig. 8 shows that hydrogen peroxide consumption (–◊–) in the presence of resorcinol sharply increased when the pH decreased below 5.7 (–△–), and this consumption was correlated with the fraction of ferrous ions in the solution (Fig. 6, –◊–) and, consequently, was related to the significant acceleration of hydroxyl radical production in homogeneous photo-Fenton processes (Eq. (1)). On the contrary, the low H_2O_2 consumption (–◊–) at pH > 5.7 (–△–) was due to the slow heterogeneous interaction of hydrogen peroxide on iron oxyhydroxide surfaces. This observation confirms that there is a transition between heterogeneous (slow) and homogeneous (fast) catalytic processes at pH ~ 5.7 during resorcinol degradation by the photo-Fenton process at circumneutral pHs. pH ~ 5.7 is achieved as a result of mixing the acidic by-products produced during resorcinol degradation, as discussed above (Section 3.2). Therefore, the pH transition (homogeneous/heterogeneous) might change depending on the organic target.

3.7. Hydrogen peroxide consumption during the photo-Fenton process at pH 7.5 in the absence of resorcinol

Fig. 9 shows the hydrogen peroxide consumption during photo-Fenton and Fenton processes in the absence of resorcinol and when the pH is maintained at 7.5 via the continuous addition of NaOH. In the photo-Fenton process, the H_2O_2 consumption at 120 min was 5, 11, 16 and 26% of that initially added, for iron concentrations of 0.7, 1.4, 2.8 and 3.1 mg L^{-1}, respectively. In contrast, the H_2O_2 consumption was only 6% in the dark Fenton process when the iron concentration was 3.1 mg L^{-1} and the H_2O_2 consumption was negligible at lower iron concentrations (data not shown).

In the absence of organic ligands that are initially present or are produced in situ from photo-Fenton degradation of a target compound, only solid iron species are present, leading to a modest consumption of H_2O_2 at pH 7.5. H_2O_2 consumption is proportional to the amount of solid iron oxyhydroxide that is suspended in the water, and the higher H_2O_2 consumption under illumination than under dark Fenton processes confirms the action of light on oxyhydroxide surfaces. Indeed, Baumgarter et al. [55] and Mazellier and Bolte [56] suggested that ferric species under illumination could be used as photo-catalysts to form reactive oxygen species (ROS), such as hydroxyl and superoxide anion radicals. Furthermore, Han et al. [57] showed that singlet oxygen ($^1O_2$) and HO• could be generated in the goethite/H_2O_2 system under room light and aerobic conditions.

3.8. Overall evolution of the photo-Fenton mechanism during the transition from circumneutral to acidic pH

From our experimental observations and an exhaustive literature review, an overall mechanism is suggested to explain the transition between heterogeneous and homogeneous photo-Fenton processes when they are used to degrade resorcinol at a circumneutral pH (Fig. 10).

In the photo-Fenton degradation of resorcinol at circumneutral pH, the transition between heterogeneous and homogeneous processes occurs as follows: (1) The formation of hydroxylated Fe^{2+} species occurs at pH values between 4.0 and 8.0 (Eqs. (4)–(6)) [33]. (2) The formation of meta-stable ferrous compounds occurs at pHs between 6.0 and 7.0 (Eq. (10)) [36]. (3) Fast oxidation by O_2 and/or H_2O_2 (Fig. 5 and Eqs. (9) and (11)) forms ferric oxyhydroxides in suspension (Fig. 6) with the concomitant generation of hydroxyl and superoxide anion radicals [33,36]. (4) The heterogeneous photo-Fenton cycle is initiated when electrons and holes are photo-generated in the iron oxyhydroxide lattice to form additional HO• [55–57]. (5) The heterogeneous photo-Fenton cycle (Figs. 8 and 9) is closed by H_2O_2 attack in an oxidative manner against Fe^{2+}, which is contained in a previously photo-reduced surface. (6) The hydroxyl and superoxide anion radicals generated in steps 3 and 5 initiate resorcinol degradation, which leads to the formation of by-products (Fig. 2c). Therefore, non-significant concentrations of soluble iron form, and low resorcinol degradation rates are the characteristics of these first (1–6) heterogeneous steps. (7) The acidic by-products (Fig. 4) play a crucial role in the transition between the heterogeneous and homogeneous photo-Fenton processes by decreasing the pH of the solution (Fig. 2) [41]. When pH 5.7 is reached, the soluble Fe^{3+} concentration is likely sufficient to form complexes with by-products, which are photo-active in the visible spectrum (Eq. (12), Fig. 7) [42]. (8) Ferric complexes are photo-activated to produce Fe^{2+}, which is the key catalyst in

homogeneous photo-Fenton processes (Fig. 6, Eq. (13)) [42–47,54]. (9) The massive and fast generation of $HO^{\bullet}$ at pH values below 5.7 (Fig. 8, —) leads to fast resorcinol degradation and mineralisation rates (step 10, Figs. 2 and 3).

4. Conclusions

When the photo-Fenton process is applied to degrade organic matter in water at circumneutral pH, degradation is favoured if siderophores are present and/or other reactions are involved. Consequently, resorcinol is the most recalcitrant of the dihydroxybenzene isomers. Resorcinol degradation through the solar photo-Fenton process is strongly dependent on pH, which determines the oxidation state and solubility of the different iron forms in the oxidative system. Above pH 5.7, the process is mainly heterogeneous and exhibits slow degradation kinetics. Below pH 5.7, the resorcinol degradation and mineralisation rates, as well as H_2O_2 consumption, are dramatically accelerated due to the increased contribution from the homogeneous process. The increase in homogeneous contribution results from the formation of aqua and organic-iron-complexes, which are excellent ROS producers that are photo-active up to 450 nm. An overall mechanistic path is proposed to illustrate the transition between heterogeneous and homogeneous photo-Fenton processes when initiated at circumneutral pH values. This transition is crucial for explaining the degradation and mineralisation rate enhancements during treatment for resorcinol and other substances.

Acknowledgments

The authors thank the Swiss National Science Foundation (SNF) and the Swiss Agency for Cooperation (DDC) for financial support within the Research partnership programme with developing countries: Project No. IZ70Z0_131312/1-2.

References

[1] F. Herrera, C. Pulgarin, V. Nadtochenko, J. Kiwi, Appl. Catal. B: Environ. 17 (1998) 141–156.
[2] G. Kleiser, F.H. Frimmel, Sci. Total Environ. 256 (2000) 1–9.
[3] G.S. Wang, S.T. Hsieh, C.S. Hong, Water Res. 34 (2000) 3882–3887.
[4] C.A. Murray, S.A. Parsons, Chemosphere 54 (2004) 1017–1023.
[5] C.S. Uyguner, M. Bekbolet, Desalination 176 (2005) 165–176.
[6] E.H. Goslan, F. Gurses, J. Banks, S.A. Parsons, Chemosphere 65 (2006) 1113–1119.
[7] S. Liu, M. Lim, R. Fabris, C. Chow, K. Chiang, M. Drikas, R. Amal, Chemosphere 72 (2008) 263–271.
[8] R.G. Zepp, B.C. Faust, J. Hoigne, Environ. Sci. Technol. 26 (1992) 313–319.
[9] C. Pulgarin, J. Kiwi, Chimia 50 (1996) 50–55.
[10] J. Bandara, C. Pulgarin, P. Peringer, J. Kiwi, J. Photochem. Photobiol. A: Chem. 111 (1997) 253–263.
[11] M. Fukushima, K. Tatsumi, S. Nagao, Environ. Sci. Technol. 35 (2001) 3683–3690.
[12] V. Sarria, S. Parra, M. Invernizzi, P. Peringer, C. Pulgarin, Water Sci. Technol. 44 (2001) 93–101.
[13] W. Gernjak, T. Krutzler, A. Glaser, S. Malato, J. Caceres, R. Bauer, A.R. Fernandez-Alba, Chemosphere 50 (2003) 71–78.
[14] W.G. Kuo, Water Res. 26 (1992) 881–886.
[15] B.C. Faust, J. Hoigne, Atmos. Environ. Gen. Top. 24A (1990) 79–89.
[16] C. Catastini, M. Sarakha, G. Mailhot, M. Bolte, Sci. Total Environ. 298 (2002) 219–228.
[17] J. Bandara, V. Nadtochenko, J. Kiwi, C. Pulgarin, Water Sci. Technol. 35 (1997) 87–93.
[18] P. Ribordy, C. Pulgarin, J. Kiwi, P. Péringer, Water Sci. Technol. 35 (1997) 293–302.
[19] F. He, L.C. Lei, J. Zhejiang Univ. Sci. 5 (2004) 198–205.
[20] M.J. Liou, M.C. Lu, J.N. Chen, Chemosphere 57 (2004) 1107–1114.
[21] S.A.O. Galvão, A.L.N. Mota, D.N. Silva, J.E.F. Moraes, C.A.O. Nascimento, O. Chiavone-Filho, Sci. Total Environ. 367 (2006) 42–49.
[22] A. Moncayo-Lasso, C. Pulgarin, N. Benitez, Water Res. 42 (2008) 4125–4132.
[23] A. Moncayo-Lasso, A.G. Rincon, C. Pulgarin, N. Benitez, J. Photochem. Photobiol. A: Chem. 229 (2012) 46–52.
[24] J. Prousek, E. Palacková, S. Priesolová, L. Marková, A. Alevov, Sep. Sci. Technol. 42 (2007) 1505–1520.
[25] A.W. Vermilyea, B.M. Voelker, Environ. Sci. Technol. 43 (2009) 6927–6933.
[26] N. De la Cruz, J. Giménez, S. Esplugas, D. Grandjean, L.F. De Alencastro, C. Pulgarín, Water Res. 46 (2012) 1947–1957.
[27] B.M. Souza, M.W.C. Dezotti, R.A.R. Boaventura, V.J.P. Vilar, Chem. Eng. J. 256 (2014) 448–457.
[28] S. Miralles-Cuevas, I. Oller, J.A.S. Pérez, S. Malato, Water Res. 64 (2014) 23–31.
[29] I. Carra, S. Malato, M. Jiménez, M.I. Maldonado, J.A. Sánchez Pérez, Chem. Eng. J. 235 (2014) 132–140.
[30] M. Minella, G. Marchetti, E. De Laurentiis, M. Malandrino, V. Maurino, C. Minero, D. Vione, K. Hanna, Appl. Catal. B: Environ. 154–155 (2014) 102–109.
[31] G. Rivas Ibáñez, J.L. Casas López, B. Esteban García, J.A. Sánchez Pérez, J. Chem. Technol. Biotechnol. 89 (2014) 1274–1282.
[32] J.M. Santana-Casiano, M. Gonzalez-Davila, F.J. Millero, Mar. Chem. 99 (2006) 70–82.
[33] B. Morgan, O. Lahav, Chemosphere 68 (2007) 2080–2084.
[34] J.M. Santana-Casiano, M. González-Dávila, A.G. González, F.J. Millero, Aquat. Geochem. 16 (2010) 467–482.
[35] J.M. Santana-Casiano, M. González-Dávila, F.J. Millero, Geochim. Cosmochim. Acta 74 (2010) 5150–5153.
[36] J.P. Jolivet, E. Tronc, C. Chanéac, C. R. Geosci. 338 (2006) 488–497.
[37] S. Malato, J. Blanco, C. Richter, P. Fernández, M.I. Maldonado, Sol. Energy Mater. Sol. Cell 64 (2000) 1–14.
[38] F. Chen, W. Ma, J. He, J. Zhao, J. Phys. Chem. A 106 (2002) 9485–9490.
[39] E. Mentasti, E. Pelizzetti, J. Chem. Soc. Dalton (1973) 2605–2607.
[40] R.C. Hider, X. Kong, Nat. Prod. Rep. 27 (2010) 637–657.
[41] L. Duczmal, A. Sobczyfiski, React. Kinet. Catal. Lett. 66 (1999) 289–295.
[42] D. Hermosilla, M. Cortijo, C.P. Huang, Chem. Eng. J. 155 (2009) 637–646.
[43] J. Garcia-Montaño, L. Perez-Estrada, I. Oller, M.I. Maldonado, F. Torrades, J. Peral, J. Photochem. Photobiol. A: Chem. 195 (2007) 205–214.
[44] W. Huang, M. Brigante, F. Wu, K. Hanna, G. Mailhot, Environ. Sci. Pollut. Res. 20 (2013) 39–50.
[45] J.H.O.S. Pereira, D.B. Queirós, A.C. Reis, O.C. Nunes, M.T. Borges, R.A.R. Boaventura, V.J.P. Vilar, Chem. Eng. J. 253 (2014) 217–228.
[46] A. De Luca, R.F. Dantas, S. Esplugas, Water Res. 61 (2014) 232–242.
[47] I.N. Diasa, B.S. Souza, J.H.O.S. Pereira, F.C. Moreira, M. Dezotti, R.A.R. Boaventura, V.J.P. Vilar, Chem. Eng. J. 247 (2014) 302–313.
[48] M. Blanco, Acta Geol. Hisp. 23 (1988) 283–290.
[49] L. Durães, B.F.O. Costa, J. Vasques, J. Campos, A. Portugal, Mater. Lett. 59 (2005) 859–863.
[50] S.K. Kwon, S. Suzuki, M. Saito, Y. Wased, Corros. Sci. 48 (2006) 3675–3691.
[51] P. Cambier, Clay Miner. 21 (1986) 191–200.
[52] D.G. Lewis, V.C. Farmer, Clay Miner. 21 (1986) 93–100.
[53] M. Kosmulski, S. Durand-Vidal, E. Maczka, J.B. Rosenholm, J. Colloid Interface Sci. 271 (2004) 261–269.
[54] J.M. Monteagudo, A. Duran, C. Lopez-Almodovar, Appl. Catal. B: Environ. 83 (2008) 46–55.
[55] E. Baumgartner, M.A. Blesa, A.H. Marinovich, A.J.G. Maroto, Inorg. Chem. 22 (1983) 2224–2226.
[56] P. Mazellier, M. Bolte, Photochem. Photobiol. Sci. 132 (2000) 129–135.
[57] S.K. Han, T. Hwang, Y. Yoon, J. Kang, Chemosphere 84 (2011) 1095–1101.